Shear-Induced Crystallization of Poly(ϵ-caprolactone). 2. Evolution of Birefringence and Dichroism

G. Floudas,*,† L. Hilliou,† D. Lellinger,‡ and I. Alig*,‡

Foundation for Research and Technology-Hellas (FO.R.T.H.), Institute of Electronic Structure and Laser, P.O. Box 1527, 711 10 Heraklion Crete, Greece, and Deutsches Kunststoff Institut, Schlossgartenstrasse 6, D-64289 Darmstadt, Germany

Received February 9, 2000; Revised Manuscript Received June 7, 2000

ABSTRACT: We have studied the crystallization of poly(ϵ-caprolactone) (PCL) with in situ optical rheometry and ex situ optical microscopy as a function of applied stress. The evolution of the birefringence and dichroism was monitored in parallel with the viscosity following a temperature jump from the melt to a final crystallization temperature for different values of stress. In optical microscopy we found an increased nucleation density which resulted in the speed-up of the crystallization process in the strained samples as detected by optical rheometry. Changes in the crystal structure observed in optical microscopy were found to correlate well with the evolution of birefringence and dichroism. An increasing volume fraction of axialites at early times and crystal branching and randomization in orientation at later times were found to control the signal from optical rheometry. A decoupling of the evolution of shear viscosity from the optical rheometry signals has been observed at high shear stress attributed to partial crystal melting. Application of a short step stress prior to crystallization is adequate to speed up the crystallization process due to the enhanced nucleation density.

I. Introduction

The problem of flow-induced crystallization is common to the industrial processing (die extrusion, injection molding) of all semicrystalline materials. Despite its technological significance and some recent experimental progress,[1−8] our current understanding of the process is relatively small. There is consensus, however, that the main effect of shear is to assist the formation of nuclei by the alignment of polymer chains in the supercooled melt. This alignment may act as a precursor for the formation of stable primary nuclei. An increasing number of such nuclei add to the stress in the system that causes further alignment of chains, thus increasing the nucleation density. The latter is probably responsible for the enhancement of the crystallization process observed experimentally.[1−8] Apart from optical microscopy studies, which probe crystal sizes typically above 1 μm, it was soon realized that more "microscopic" techniques are needed to probe the chain stretching and orientation prior to crystallization.

Since the early work of Stein and co-workers,[9] birefringence and in some cases dichroism have been employed to follow the chain orientation and crystallization of polymers subjected to flow fields. The polymers were mainly polyethylene (PE), poly(ethylene terephthalate) (PET), and polypropylene (PP). McHugh and co-workers[10,11] employed simultaneous measurements of birefringence and dichroism to study the crystallization of high-density PE melt subjected to planar extensional flow. Following a short interval of flow two maxima have been detected in the birefringence intensity: one due to flow-induced deformation and a second due to oriented crystallization. By moving to regions of higher orientation the second process gained intensity and moved to shorter times. A quantitative measure of the crystallization rate revealed an acceleration by orders of magnitude as compared to the quiescent state. Combined birefringence and infrared dichroism measurements have also been employed in linear PE in an attempt to reevaluate the intrinsic amorphous birefringence[12] which was found to be about 0.06. Furthermore, the stress overshoots in the flow-induced birefringence of branched polyethylene melts were attributed to molecular stretching.[13]

The elongational flow-induced crystallization of PET was studied[14] as well as the validity of the stress−optical relationship under uniaxially stretched PET.[15] In the latter study, the onset of crystallization was detected from the deviation of the stress−birefringence curve from the stress−optical rule.

The transient birefringence of polydisperse isotactic polypropylene revealed contributions from chain stretching and from highly oriented structures during shear.[16] A brief interval of shear could reduce the crystallization times by 2 orders of magnitude. In addition, recent simultaneous measurements of birefringence and dichroism allowed the isolation of the isotactic and atactic populations within the elastomeric PP.[17]

In the single study[18] on poly(ϵ-carpolactone) (PCL) the strain-induced crystallization was studied by infrared dichroism in its miscible blends with poly(vinyl alcohol). It was found that crystallization under strain lead to different crystalline orientations: perpendicular and parallel to the strain direction at low and high draw ratios, respectively.

In our previous study,[19] we have investigated the effect of shear rate on the crystallization of PCL and were able to separate the effect of thermally driven from strain-induced crystallization. The effect of increasing shear rate was to lower the free enthalpy barrier required for the formation of a stable nucleus. The lower barrier resulted in the enhancement of the nucleation density and eventually in the speed-up of the crystallization process. In the present study we employ optical rheometry (in situ birefringence and dichroism) and

† Institute of Electronic Structure and Laser.
‡ Deutsches Kunststoff Institut.

10.1021/ma000243b CCC: $19.00
Published on Web 08/01/2000

Scheme 1

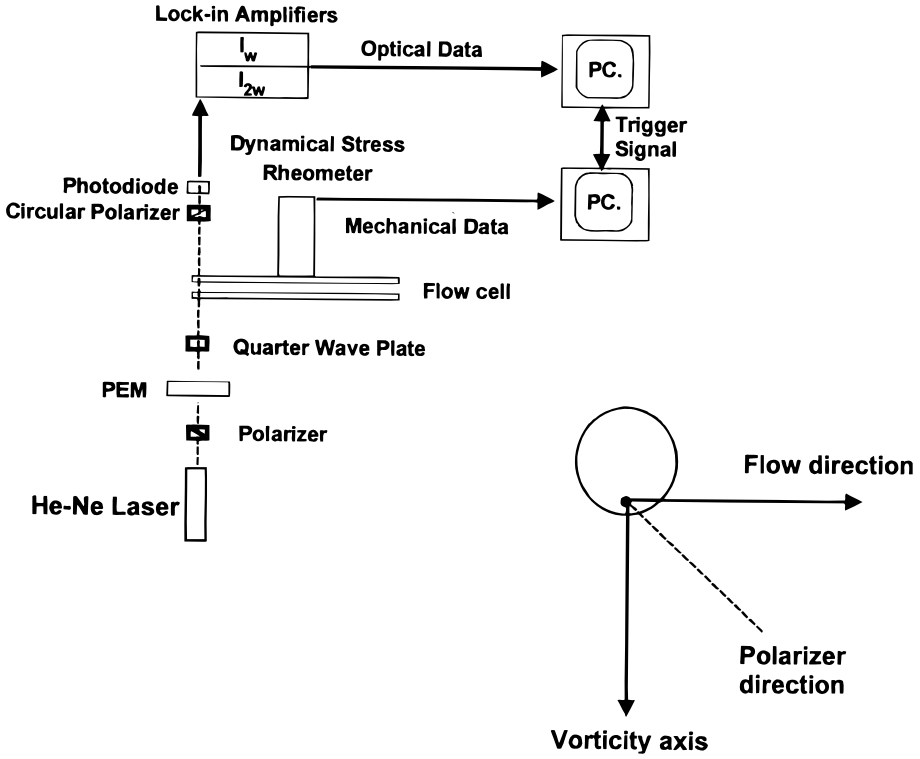

rheology with ex situ microscopy which provide direct information on the morphological changes occurring during the stress-induced crystallization of PCL. The signal from optical rheometry is controlled by two competing factors: an increasing volume fraction of crystals at short times and by processes which reduce the optical anisotropy at later times. The intensity and time dependence of the birefringence and dichroism signals were found to have a strong dependence on the applied stress which is rationalized in terms of morphological changes during PCL crystallization.

II. Experimental Section

Sample. The PCL homopolymer (Aldrich) was synthesized by anionic polymerization following standard procedures and kindly provided by Dr. G. Reiter (CNRS, Mulhouse). The sample had a number-averaged molecular weight of 1×10^4 and a polydispersity of 1.4.

Optical Rheometry. A Rheometric Scientific constant stress rheometer (DSR-200) with a controlled strain option was coupled to an optical analyzer which allowed simultaneous measurements of the viscoelastic and optical properties (birefringence and dichroism) of the semicrystalline polymer. Details of the measurement technique can be found elsewhere.[20] A schematic representation of the experimental setup is shown in Scheme 1.

The sample is contained between two quartz disks (38.1 mm in diameter) that form a parallel plate shear cell with a separation of 0.5 mm. The upper plate is rotated to induce shear. Temperature control is achieved with the original DSR circulating fluids (ethylene glycol/water mixture) bath, which was appropriately modified in order to fit in the optical train, allowing the laser beam to pass through. The optical train is composed of a He−Ne laser (wavelength of 632.8 nm) followed by a polarizer oriented at −45° with respect to the flow direction. A photoelastic modulator (PEM) (Hinds Instruments Inc.), oriented along the flow, induces a sinusoidally varying retardance, δ, to the phase of the transmitted light, according to $\delta = A \sin(\omega t)$, where A is an adjustable experimental parameter, ω is a fixed frequency of 50 kHz, and t is the time. The modulated beam is then transmitted through a quarter-wave retarder, oriented at −45°. The light exiting the optical train is linearly polarized, with the polarization direction oscillating between 45° and −45° relative to the polarizer at 50 kHz. The light is then passed through the flow cell. The exiting beam is either passed through a circular polarizer and then collected at the photodiode (in a birefringence experiment) or simply collected at the photodiode (in a dichroism experiment). The role of the circular polarizer is to transform all elliptically or circularly polarized light into linearly polarized which is required for the determination of the anisotropy in the retardation of light. In the case of dichroism, the type of polarization is not important since we are looking for anisotropy in the intensity and not in the phase of light. The resulting modulated intensity in either case is of the form

$$I = I_{dc} + I_\omega \sin(\omega t) + I_{2\omega} \cos(2\omega t) + ... \quad (1)$$

The use of lock-in amplifiers set at reference frequencies corresponding to ω and 2ω allows the determination of the Fourier coefficients, I_ω and $I_{2\omega}$, which are functions of the birefringence or dichroism. Ratios, R^D_ω, $R^D_{2\omega}$, R^B_ω, and $R^B_{2\omega}$, of each Fourier coefficient to the appropriate mean intensity (I^D_{dc} or I^B_{dc}) are formed in order to account for turbidity changes and random fluctuations in the light source. The experiment produces the following ratios for the dicroism:

$$R^D_\omega = \frac{I^D_\omega}{2I^D_{dc}J_1(A)} = -\sin(2\theta'') \tanh \delta''$$

$$R^D_{2\omega} = \frac{I^D_{2\omega}}{2I^D_{dc}J_2(A)} = -\cos(2\theta'') \tanh \delta'' \quad (2)$$

and for the birefringence

$$R^B_\omega = \frac{I^B_\omega}{2I^B_{dc}J_1(A)} = -\cos(2\theta') \sin \delta' - \sin(2\theta'') \tanh \delta''$$

$$R^B_{2\omega} = \frac{I^B_{2\omega}}{2I^B_{dc}J_2(A)} = \sin(2\theta') \sin \delta' - \sin(2\theta'') \tanh \delta' \quad (3)$$

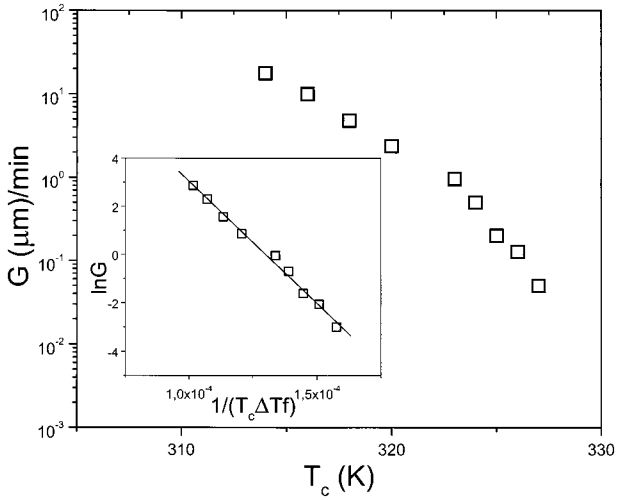

Figure 1. Growth rates of axialites obtained from optical microscopy plotted as a function of crystallization temperature. In the inset the same growth rates are plotted as a function of reduced temperature (see text).

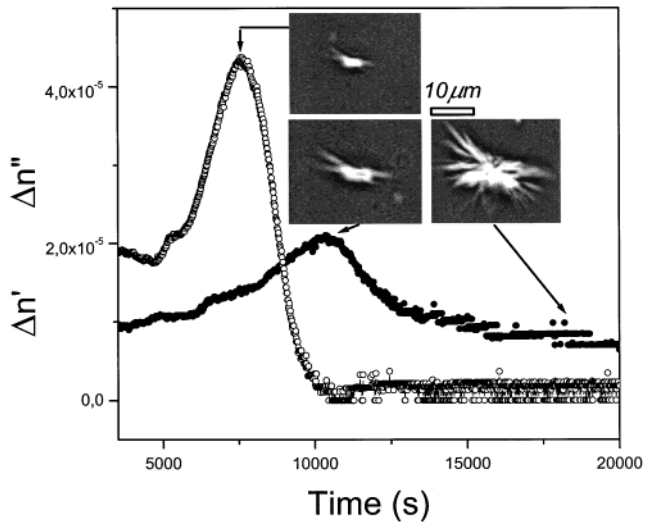

Figure 2. Time evolution of the birefringence $\Delta n'$ (open symbols) and dichroism $\Delta n''$ (filled symbols) following a temperature jump from 353 to 328 K. The insets are optical micrographs obtained ex situ after $t_1 = 7300$ s, $t_2 = 9500$ s, and $t_3 = 19\,900$ s. The bar indicates a length of 10 μm.

where $J_1(A)$ and $J_2(A)$ are Bessel functions, θ' is the orientation angle of the birefringence, δ' is the retardance of the light, θ'' is the orientation angle of the dichroism relative to the polarizer direction, and δ'' is the extinction of the light. The above parameters were measured during the crystallization experiments (see below). The birefringence $\Delta n'$ is related to the retardation by $\delta' = 2\pi d\Delta n'/\lambda$, where d is the sample thickness and λ is the wavelength of light, whereas the dichroism is related to the extinction by $\delta'' = 2\pi d\Delta n''/\lambda$. To properly determine the birefringence and dichroism, the Bessel functions must be calculated. This calibration was accomplished by rotating a polarizing strip in the sample position and calculating appropriate Bessel function values. The evolution of the orientation angles and of the birefringence and dichroism signals is discussed below.

Optical Microscopy (OM). A Zeiss Axioskop 2 polarizing optical microscope was used together with a Linkam heating stage (THMS 600) and a TP93 temperature programmer (heating and cooling rates of 0.1−90 K/min). We have followed the growth of crystals in real time by a continuous recording using a CCD camera ($^1/_2$ in. SONY color camera) and a fast frame grabber (capable of up to 50 frames/s). The analysis in terms of the nucleation density, shape, and growth rates was made with an appropriate software (Image Pro Plus). The experiments on the unstrained sample were made by heating to an initial temperature of 353 K following quenches to different crystallization temperatures. The strained samples prepared in the rheometer were quenched to liquid nitrogen and transferred to the microscope.

III. Results and Discussion

Thermally Induced Crystallization. First, we studied the crystallization process in the unstrained melt using polarizing optical microscopy (OM). With OM we followed the linear growth rates at the different crystallization temperatures (in the range from 314 to 327 K) following quenches from an initial temperature of 353 K, and the result is shown in Figure 1. PCL is known[21] to form axialites at short times which at longer times become spherulitic due to crystal branching. As we will see below, it is exactly this property of the superstructure which make the system a unique one for monitoring the birefringence and dichroism evolution. In the inset to Figure 1 the same growth rates are plotted as a function of the crystallization temperature T_c, the degree of supercooling ($\Delta T = T_m^o - T_c$, where $T_m^o = 346$ K is the equilibrium melting temperature[21]), and f is a temperature correction factor ($= 2T_c/(T_m^o + T_c)$). At the crystallization temperature of 328 K, the growth rate is very small, but an estimate can be provided by the linear extrapolation of Figure 1. Using the extrapolated value of G and assuming a linear growth rate (i.e., $R = Gt$, where R is the radius), we obtain a size of 0.3 μm at $t = 1000$ s. This implies that the features of the birefringence and dichroism obtained during the kinetic experiments (below) refer to structures larger than 0.3 μm.

The evolution of birefringence ($\Delta n'$) and dichroism ($\Delta n''$) following a temperature jump from 353 to 328 K is shown in Figure 2 under quiescent conditions. The final crystallization temperature ($T = 328$ K) was carefully chosen, so that the crystallization process initiated after the T equilibration for both the strained and unstrained cases. As seen in Figure 2, both $\Delta n'(t)$ and $\Delta n''(t)$ display a bell-like shape with maxima shifted on the time axis. The orientation angles θ' and θ'' (not shown here) revealed that the birefringence and dichroism signals originate from structures oriented near to the vorticity axis (Scheme 1). Measurements of these quantities have been repeated several times for the same quench depth, and the form of $\Delta n'(t)$ and $\Delta n''(t)$ was found to be invariant. If only few axialites are within the laser beam which give rise to the observed birefringence and dischroism, then, depending on the orientation angles θ' and θ'', different signs of $\Delta n'(t)$ and $\Delta n''(t)$ are to be expected. Then the consistency of the data in Figure 2 imply some preoriented structures mainly along the vorticity direction by the sample preparation method (radial flow of sample during preparation or thermal gradient). It is worth mentioning here that similar features to the ones shown in Figure 2 (with the bell-like birefringence) have been seen in the flow-induced crystallization of high-density PE subjected to an elongational flow.[10,11]

Optical micrographs (taken ex situ) are shown which are obtained during the thermally induced crystallization process and reveal structural changes on a length scale of 1−10 μm. The birefringence has contributions from intrinsic and form effects and is in general sensitive to smaller length scales than the dichroism which

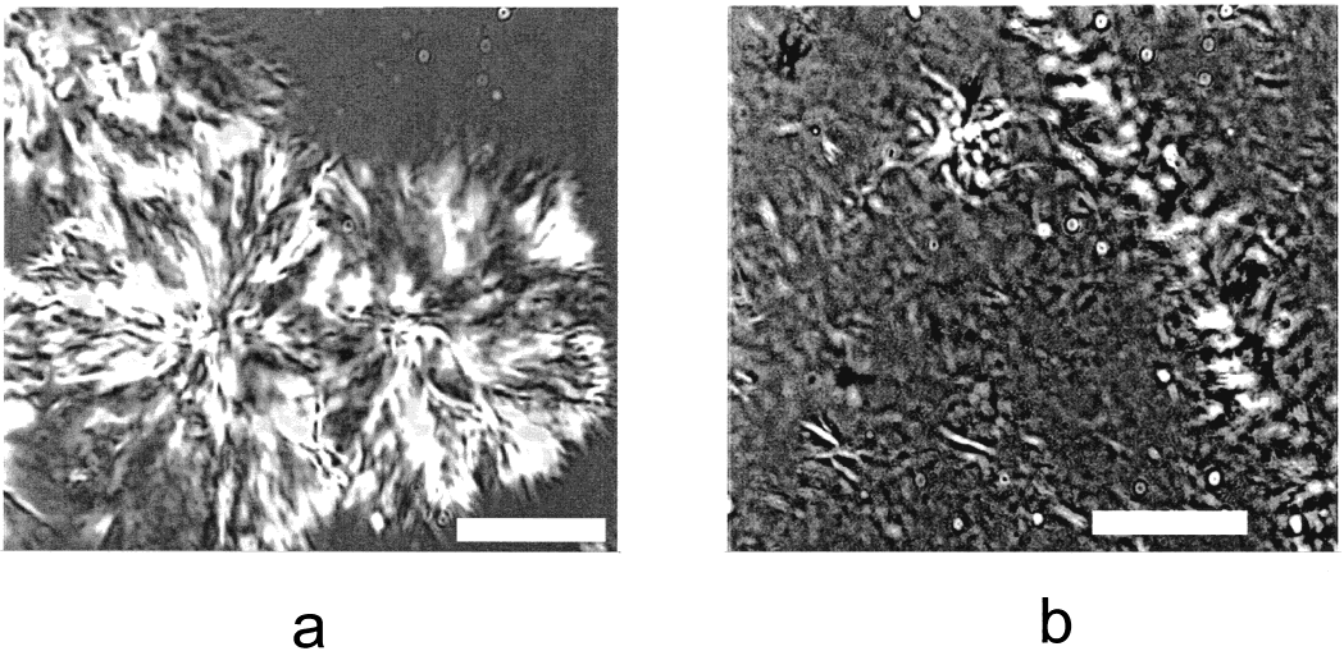

Figure 3. Optical micrographs of two samples. The first image (a) corresponds to a sample quenched from 353 to 328 K without any shear (thermally induced nucleation). The second image (b) is taken from a sheared sample (τ = 500 Pa) with the same thermal history as the first one. Notice the increased number and smaller size of nuclei. The bar indicates a characteristic distance of about 50 μm.

contains contributions only from the latter. Then the evolution shown in Figure 2 can be understood with the help from the optical micrographs. The optical micrographs show an increasing number of nuclei of axialitic shape for short times, with crystal branching starting at about 7×10^3 s. Symmetric branching starts at about 1×10^4 s, and at longer times a nearly spherulitic superstructure is formed. The bell-shaped birefringence can be understood as follows: The birefringence of semicrystalline polymers is given by

$$\Delta n' = \Delta n_{\text{intr}} + \Delta n_{\text{form}} \tag{4}$$

where Δn_{intr} and Δn_{form} are the intrinsic and form contributions, respectively. For the intrinsic part, additivity of the crystalline and amorphous contributions is usually assumed:

$$\Delta n_{\text{intr}} = \varphi_c f_c \Delta n_c + (1 - \varphi_c) f_a \Delta n_a \tag{5}$$

where φ_c and φ_a (= $1 - \varphi_c$) are the volume fractions of the crystal and amorphous phases, f_c and f_a are the crystalline and amorphous orientation functions ($f = {}^3/_2\langle\cos^2\theta\rangle - {}^1/_2$), and Δn_c and Δn_a are the intrinsic birefringence values for the perfectly oriented crystalline and amorphous phases. The form birefringence (Δn_{form}) is proportional to $\varphi_c F$, where F is a "shape factor" measuring the departure from a spherical overall shape.

The evolution of $\Delta n'(t)$ is dominated by the intrinsic contribution of the crystal phase, i.e., $\Delta n'(t) \approx \varphi_c(t) f_c(t) \Delta n_c$, with a competition between an increasing volume fraction of crystals at short times followed by asymmetric branching (which creates a birefringence on a smaller length scale) and possibly by the loss of orientation of axialites at longer times. These antagonistic factors create a maximum in the evolution of $\Delta n'(t)$ whose location on the time axis provides a qualitative measure of the course of crystallization. On the other hand, the dichroism contains only form effects, i.e., $\Delta n''(t) = \Delta n_{\text{form}}(t) \approx \varphi_c(t) F(t)$, and the bell shape is created by the competition between an increasing volume fraction at short times and a lower overall anisotropy at longer times. The small final anisotropy can result from both loss of the anisotropic shape and by the randomization of the axialitic orientation. Notice that at $t = 10^4$ s $\Delta n'$ is nearly zero, but $\Delta n''$ is at its maximum value. One way of explaining this difference is by the symmetric branching starting at this time which creates a low $\Delta n'$ value. However, the overall shape is still asymmetric, leading to the form anisotropy detected by the $\Delta n''$. Alternatively, the birefringence contains antagonistic interactions between intrinsic and form effects whereas the dichroism contains only form effects.

Stress-Induced Crystallization. The major effect of applied stress is to increase the nucleation density. This is shown in Figure 3 where optical micrographs from an unstrained and a strained sample are compared. The first image (a) corresponds to a sample quenched from 353 to 328 K without any stress, i.e., thermally induced nucleation (in situ microscopy). The second image (b) is taken from a sample quenched from 353 to 328 K but under continuous shearing conditions (τ = 500 Pa) (ex situ). The latter image shows many axialites and in parts row nucleation. There is a 30-fold increase in the nucleation density in (b) as a result of the applied stress. This increase in the nucleation density has profound effects on the crystallization kinetics. In Figure 4 the transmitted intensity, I_{dc}, is plotted during the kinetic experiments (from 353 to 328 K) for different levels of stress. The transmitted intensity decreases with time as a result of the growing turbidity in the sample. Notice that the signal at long times does not decay to zero but to a value between 0.1 and 0.2, reflecting mainly scattered light which is getting through the sample. The intensity decays faster with increasing level of applied stress, meaning that the

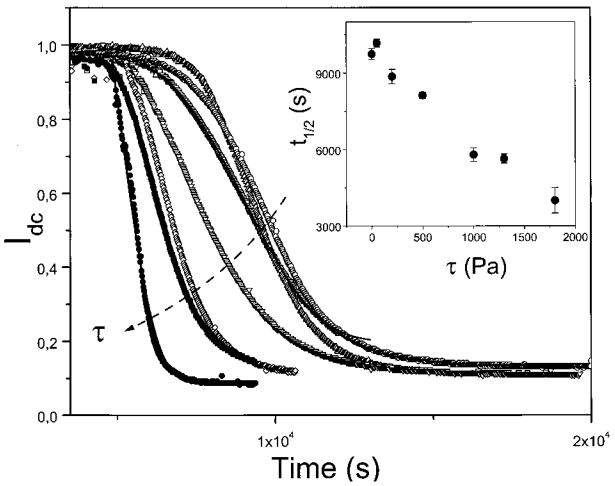

Figure 4. Transmitted intensity I_{dc} measured during the dichroism experiments following temperature jumps from 353 to 328 K. The different curves correspond to the different levels of stress applied continuously during the experiments: (○) 0, (△) 50, (□) 200, (▽) 500, (◇) 1000, (■) 1300, and (●) 1800 Pa. In the inset, the characteristic kinetic times $t_{1/2}$, obtained using the Avrami analysis, are plotted as a function of applied stress. The lines for the 200 and 1800 Pa cases are the result of the fit to the Avrami equation.

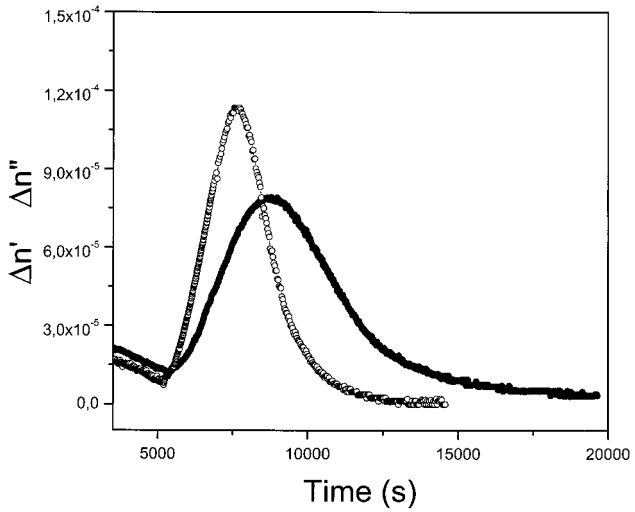

Figure 5. Time evolution of the birefringence $\Delta n'$ (open symbols) and dichroism $\Delta n''$ (filled symbols) following a temperature jump from 353 to 328 K with a stress of 500 Pa. Notice the higher magnitude of both quantities as compared to the unstrained case (Figure 2).

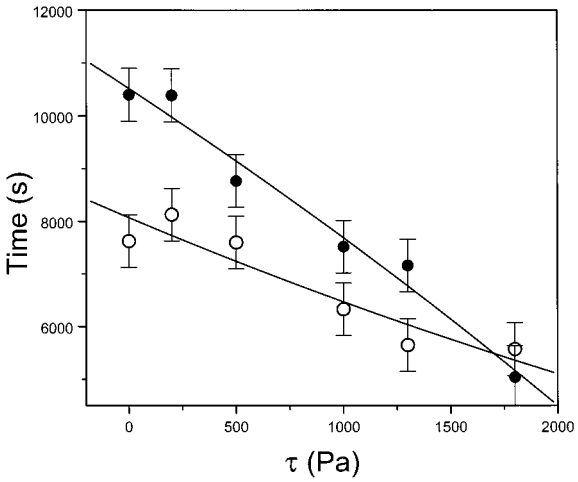

Figure 6. Characteristic times corresponding to the birefringence (open symbols) and dichroism (filled symbols) maxima plotted as a function of stress. All times refer to crystallization at 328 K.

whole process speeds up. We have used the Avrami equation[22]

$$1 - \varphi_c(t) = e^{-z(t-t_0)^n} \qquad (6)$$

for the evaluation of the degree of crystallinity where z is a rate constant, n is the Avrami exponent, and t_0 is a delay which takes into account the equilibration time to the final crystallization temperature. We have further assumed that the volume fraction of the crystalline phase $\varphi_c(t)$ is proportional to the extinction of light in the sample. We therefore calculated $\varphi_c(t)$ using $\varphi_c(t) = -k \ln(I_{dc}(t)/I_{dc}(0))$, where k is a constant and $I_{dc}(t)$ is the observed light intensity. The constant k is calculated from the final crystallinity and the intensity value at $t \rightarrow \infty$ as $k = -\varphi_c(\infty)/\ln(I_{dc}(\infty)/I_{dc}(0))$. For $\varphi_c(\infty)$ and $I_{dc}(\infty)$, we have used the values of 67% (obtained from DSC) and 0.13 (from Figure 4), respectively. The characteristic times, $t_{1/2} = (\ln 2/z)^{1/n}$, are plotted in the inset as a function of applied stress. At the maximum applied stress the crystallization time is reduced by a factor of 2 relative to the quiescent case. The Avrami exponent, reflecting the dimensionality and nature of the nucleation and growth process, varies from 3.2 to about 8 at 1800 Pa. The former value can be rationalized in terms of the Avrami theory; however, the latter is much too high as have been observed in the past.[23]

Figure 5 gives the evolution of the birefringence and dichroism for the same T-jump but with a stress of 500 Pa. The bell shape of $\Delta n'(t)$ and $\Delta n''(t)$ is preserved and originates from an increasing volume fraction at short times and by the loss of internal anisotropy and by the randomization in the orientation of the increased in numbers axialites at longer times as indicated by the orientation angles. However, both curves show profound differences from the corresponding ones for the unstrained case (Figure 2). First, both maxima are shifted to shorter times, indicating the speed-up of the process and second the signals are enhanced. To quantify the effect of the stress on the crystallization process, at least in a qualitative way, we use the times corresponding to the maxima of the birefringence and dichroism. This is shown in Figure 6, where the above times are plotted as a function of the applied stress. The speed-up of the crystallization process is the result of the increased nucleation density with applied stress (Figure 3). A speed-up similar to the one shown in Figures 5 and 6 has been seen during the flow-induced crystallization of high-density PE subjected to an elongational flow.[10,11] Following the cessation of flow two processes have been detected in the birefringence signal: a fast one related to flow-induced deformation and a slower one related to the oriented crystallization. The latter process was found to depend strongly on the flow field. The absence of the former process in our experiments is simply because of interference with the temperature stabilization effects.

In parallel with the optical measurements, we have followed the evolution of the viscosity, and the result is shown in Figure 7 for the different stress values. In all curves there is an "incubation period" followed by a rapid viscosity increase at longer times. Within the "incubation period" there exist axialites of micrometer

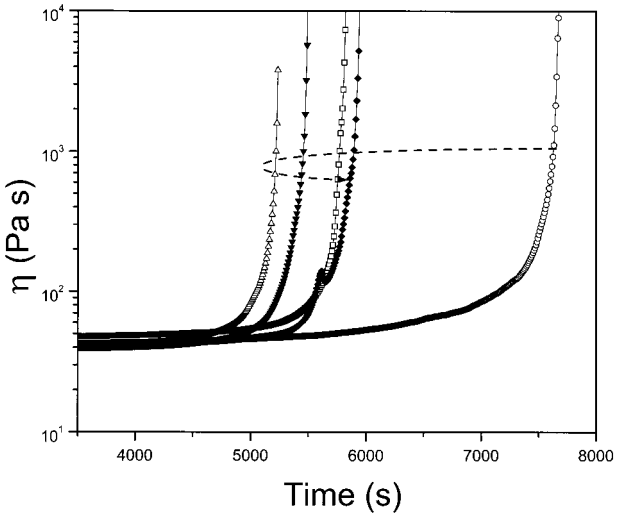

Figure 7. Evolution of viscosity measured during the birefringence experiments following a temperature jump from 353 K to the same crystallization temperature (328 K) shown for different stress values: (○) $\tau = 50$ Pa, (□) $\tau = 200$ Pa, (△) $\tau = 500$ Pa, (▼) $\tau = 1000$ Pa, and (◆) $\tau = 1800$ Pa. Notice the reversal in the $\eta(t)$ behavior at $\tau = 500$ Pa.

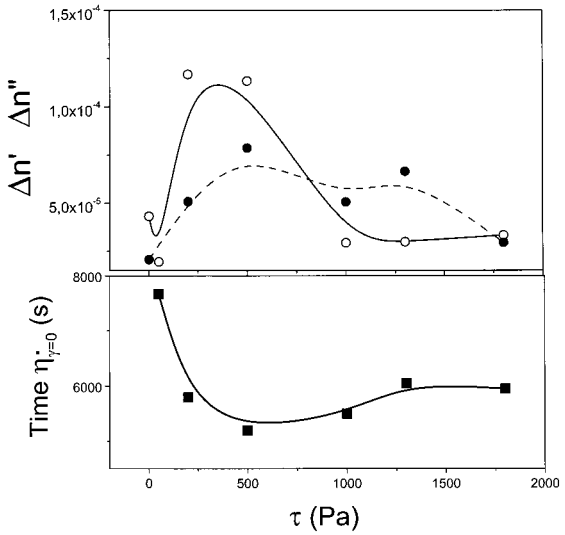

Figure 8. (top) Dependence of the birefringence (filled symbols) and dichroism (open symbols) maxima obtained during the kinetic experiments on the applied stress. (bottom) Time corresponding to the viscosity at zero shear rate as obtained from the divergence of the viscosity curves of Figure 7, plotted as a function of shear stress. The data imply a correlation of the $\Delta n'$ and $\Delta n''$ maximum values with the $\eta(t)$ reversal of Figure 7.

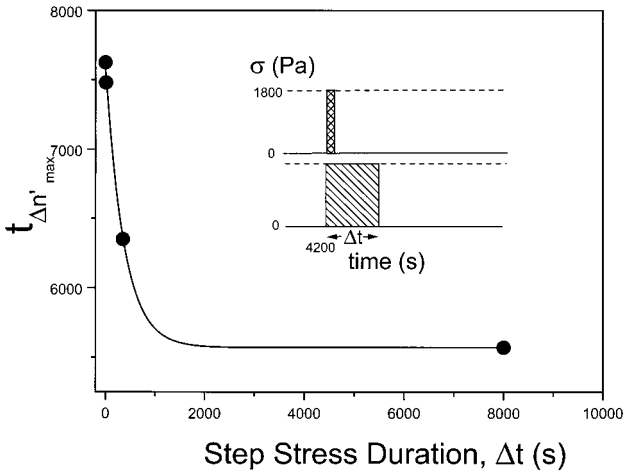

Figure 9. Characteristic times corresponding to the birefringence maximum during the kinetic experiments (from 353 K to the crystallization temperature of 328 K) plotted as a function of the step stress period at the initial stages of crystallization. The stress level was 1800 Pa, and the point at 8000 s corresponds to a continuously sheared sample. Notice that a step stress in the undercooled melt for 350 s is enough to initiate the crystallization process.

size which can flow and do not influence considerably the overall viscosity. The sharp increase in viscosity at longer times ($\eta_{\dot\gamma\to 0}$) is due to the presence of crystals which are formed first in the periphery of the plates (where the maximum strain is applied) and result practically in an infinite viscosity (when the shear rate goes to zero). Notice that the time where $\eta_{\dot\gamma\to 0}$ is obtained is decoupled from the $\Delta n'$ and $\Delta n''$ maxima since the viscosity is mainly controlled by the crystals formed at the outermost part of the sample whereas the latter are measured at half the maximum strain (i.e., in the middle of the plates). Furthermore, there is a peculiar reversal in the behavior of $\eta(t)$ with increasing stress: for small stresses, increasing stress speeds up the viscosity upturn whereas at higher stresses this feature is retarded. The reversal at high stresses might be caused by destruction of the crystals formed in the periphery. This phenomenon might be related to the shear melting of colloidal crystals above a critical shear stress.[24] Alternatively, shear thinning due to improved orientational order with increasing stress can also cause the reversal seen in Figure 7. To distinguish between the two possibilities, we compare the characteristic times corresponding to $\eta_{\dot\gamma\to 0}$ with the birefringence and dichroism peak values as a function of applied stress in Figure 8. The reversal of the time dependence of the viscosity curves finds its counterpart in the decrease of the birefringence and dichroism peak values, indicating a possible correlation of the changes in the viscoelastic properties with the optical properties due to the partial destruction of the superstructure (shear melting).

In a last series of experiments we have investigated the effect of a step stress on the crystallization kinetics applied at the final crystallization temperature. For this purpose we have applied a step stress of 1800 Pa for short times (short meaning shorter than the evolution of the crystallization process with duration of 10, 150, and 350 s) corresponding to the "incubation period". As in the corresponding experiments under continuous shearing, we found that the crystallization process speeds up. This is depicted in Figure 9 where we plot the time corresponding to the birefringence maximum as a function of the step stress duration. There is a clear speed-up of the process; a step stress of 350 s duration can speed up the crystallization process by 1000 s. The enhanced crystallization process is consistent with the increased nucleation density observed in optical microscopy (Figure 3) and shows that the nucleation process is greatly affected by short-time shearing at the final crystallization temperature in the supercooled melt state. The energy provided by the stress is given to orient the chains and possibly alters the conformation to trans sequences. This finding is of importance in polymer crystallization during processing and should be considered in future simulations of flow-induced crystallization.

IV. Conclusions

We have employed in situ optical rheometry with ex situ optical microscopy to investigate the influence of stress on the crystallization kinetics of PCL. PCL like PE crystallize in an orthorhombic unit cell and form superstructures whose shape is a function of the crystallization time, temperature, and shear rate. The main conclusions of the present study can be summarized as follows:

1. The evolution of birefringence and dichroism following a temperature jump from the melt display maxima that can be rationalized by an increasing volume fraction of axialites at early times and by the loss of optical anisotropy (crystal branching resulting in loss of shape anisotropy and randomization in axialitic orientation) at later times.

2. A decoupling of the shear viscosity from the optical rheometry features has been observed at high shear stresses and attributed to partial melting of crystals.

3. Short-term stress applied before the onset of crystallization is adequate to speed up the crystallization process due to the enhanced nucleation density.

This work has left several open questions that need to be addressed in the future. For example, the effect of crystal orientation on the evolution of birefringence and dichroism need to be explored in detail. Furthermore, the long times associated with temperature equilibration precluded a study of the chain orientation process. The high Avrami exponents at the high stress values call also for an explanation. The above together with the more fundamental questions as to the role of entanglements and to the main variable (stress, strain, strain rate) controlling flow-induced crystallization will be addressed in future studies.

Acknowledgment. This work was supported by the Greek Secretariat for Research and Technology (GGET) by a grant (99ED95) and by the Alexander von Humboldt Stiftung. D.L. and I.A. thank the "Bundesministerium fur Bildung und Forschung" (BMBF) for the financial support (Grant 03N5018H7). We thank Prof. G. Fuller for many illuminating discussions and comments.

References and Notes

(1) Eder, G.; Janeschitz-Kriegl, H.; Liedauer, S. *Prog. Polym. Sci.* **1990**, *15*, 629.
(2) Jerschow, P.; Janeschitz-Kriegl, H. *Int. Polym. Proc.* **1997**, *1*, 72.
(3) Peterlin, A. In *Flow Induced Crystallization*; Miller, R. L., Ed.; Gordon: New York, 1979.
(4) Larsen, A.; Hande, O. *Colloid Polym. Sci.* **1993**, *271*, 277.
(5) Wolkowitz, M. D. *J. Polym. Sci., Polym. Symp.* **1978**, *63*, 365.
(6) Tribout, C.; Monasse, B.; Haudin, J. M. *Colloid. Polym. Sci.* **1996**, *274*, 197.
(7) Duplay, C.; Monasse, B.; Haudin, J. M.; Costa, J. L. *Polym. Int.* **1999**, *48*, 320.
(8) Monasse, B. *J. Mater. Sci.* **1995**, *30*, 5002.
(9) Stein, R. S. *Newer Methods in Polymer Characterization*; Wiley-Interscience: New York, 1964.
(10) McHugh, A. J.; Guy, R. K.; Tree, D. A. *Colloid Polym. Sci.* **1993**, *271*, 629.
(11) Bushman, A. C.; McHugh, A. J. *J. Appl. Polym. Sci.* **1997**, *64*, 2165.
(12) Rossignol, J. M.; Sequela, R.; Rietsch, F.; Dupuis-Lallemand *J. Polym. Sci., Polym. Phys. Ed.* **1989**, *27*, 527.
(13) Chai, C. K.; Creissel, J. Randrianantoandro *Polymer* **1999**, *40*, 4431.
(14) Kubo, H.; Okamoto, M.; Kotaka, T. *Polymer* **1998**, *39*, 4827; **1998**, *39*, 501.
(15) Ryu, D. S.; Inoue, T.; Osaki, K. *Polymer* **1998**, *39*, 2515.
(16) Kumaraswamy, G.; Issaian, A. M.; Kornfield J. A. *Macromolecules* **1999**, *32*, 7537.
(17) Carlson, E. D.; Fuller, G. G.; Waymouth, R. M. *Macromolecules* **1999**, *32*, 8100.
(18) Zhao, Y.; Keroack, P.; Prud homme, R. *Macromolecules* **1999**, *32*, 1218.
(19) Lellinger, D.; Floudas, G.; Alig, I. *Macromolecules*, submitted.
(20) Fuller, G. G. *Optical Rheometry of Complex Fluids*; Oxford University Press: New York, 1995.
(21) Floudas, G.; Reiter, G.; Lambert, O.; Dumas, P. *Macromolecules* **1998**, *31*, 7279.
(22) Avrami, M. J. *J. Chem. Phys.* **1939**, *7*, 1103; **1940**, *8*, 212; **1941**, *9*, 177.
(23) Sherwood, C. H.; Price, F. P.; Stein, R. S. *J. Polym. Sci., Polym. Symp.* **1978**, *63*, 77.
(24) Imhof, A.; van Blaaderen, A.; Dhont, J. K. G. *Langmuir* **1994**, *10*, 3477.

MA000243B